

Floor Plan-Guided Visual Navigation Incorporating Depth and Directional Cues

WeiQi Huang¹, Jiaxin Li¹, Zan Wang¹, Huijun Di¹, Wei Liang^{1,2,†}, Zhu Yang¹

Abstract—Current visual navigation strategies mainly follow an exploration-first and then goal-directed navigation paradigm. This exploratory phase inevitably compromises the overall efficiency of navigation. Recent studies propose leveraging floor plans alongside RGB inputs to guide agents, aiming for rapid navigation without prior exploration or mapping. Key issues persist despite early successes. The modal gap and content misalignment between floor plans and RGB images necessitate an efficient approach to extract the most salient and complementary features from both for reliable navigation. Here, we propose *GlocDiff*, a novel framework that employs a diffusion-based policy to continuously predict future waypoints. This policy is conditioned on two complementary information streams: (1) local depth cues derived from the current RGB observation, and (2) global directional guidance extracted from the floor plan. The former handles immediate navigation safety by capturing surrounding geometry, while the latter ensures goal-directed efficiency by offering definitive directional cues. Extensive evaluations on the FloNa benchmark demonstrate that *GlocDiff* achieves superior efficiency and effectiveness. Furthermore, its successful deployment in real-world scenarios underscores its strong potential for broad practical application.

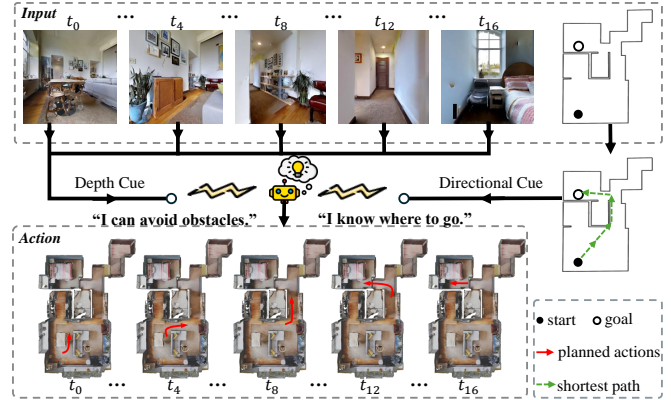


Fig. 1. At each time step, our method extracts the depth cue from the observation frames and derives the directional cue by planning the shortest path to the goal on the floor plan. Both complementary cues facilitate the learning of a navigation policy that integrates obstacle avoidance with efficient goal-reaching behavior.

I. INTRODUCTION

Indoor visual navigation has long been a prominent topic in embodied AI research, fostering a wide range of downstream applications, including emergency rescue, assistive robotics, and autonomous exploration. At its core, the task requires agents to navigate through diverse, previously unseen environments toward specified goals using visual observations. These observations, often in the form of RGB or RGB-D images, provide only limited egocentric views of the environment, thereby constraining the agent’s ability to plan globally optimal and efficient paths.

To address this limitation, recent work [1–5] has increasingly explored integrating prior floor plans with visual inputs. Floor plans constitute a valuable and widely available source of global spatial knowledge, providing high-level semantic and geometric layouts that remain invariant to dynamic changes such as temporary obstacles or furniture rearrangement. This inherent stability makes them well-suited as priors for supporting navigation in unseen environments.

However, effectively integrating these two data sources for both local obstacle avoidance and global path planning remains challenging. The main bottleneck is the inherent mismatch between them: (1) a difference in the way spatial information is represented in egocentric observations versus abstract top-down architectural plans, and (2) a content gap,

where objects (e.g., furniture) present in observations are missing from the static floor plan. While prior approaches bypass this challenge by establishing extra topological or semantic maps, combining them with perceptions from LiDAR [1, 2] and inertial measurement units [6], they also introduce increased system costs. Li et al. [3] employ a unified image encoder to extract latent features from both floor plans and visual observations, followed by transformer-based fusion for action prediction. This method achieves only a superficial and ineffective fusion. By processing the floor plan as a mere image, it squanders the inherent, explicit representation of global connectivity that is the defining feature of a human-abstracted topological map.

We propose *GlocDiff*, a diffusion-based policy for floor plan-guided visual navigation. The core idea of *GlocDiff* lies in leveraging depth and directional cues from RGB observations and the floor plan, respectively, to guide action generation. As shown in Fig. 1, *GlocDiff* bridges the representational gap by extracting a sequence of 2D waypoints (the shortest path) from the floor plan’s topology. This path—despite potential obstacle intersections—provides a geometrically grounded directional prior, translating the abstract map into actionable sub-goals for egocentric control. Concurrently, *GlocDiff* complements the global path with fine-grained local geometry. It leverages a depth encoder [7] to produce depth features from RGB observations, which reveal traversable regions and obstacles absent from the floor plan. To synthesize smooth and temporally coherent action

¹Beijing Institute of Technology, ²Yangtze Delta Region Academy of Beijing Institute of Technology, [†]indicates the corresponding author.

sequences from these complementary signals, we employ a conditional diffusion model. It is conditioned on both guidance sources and trained to generate actions by supervised learning on optimal trajectories. To enhance robustness against the inevitable localization errors known to impact navigation performance [1, 3], we incorporate Gaussian noise perturbations into the agent’s pose and path planning results during training. Consequently, *GlocDiff* can be effectively deployed with a standard VO module [8], achieving robust performance even when faced with its noisy pose estimates.

Extensive experiments on the FloNa [3] benchmark demonstrate that our approach outperforms the baselines even with fewer training pairs, emphasizing its effectiveness and data efficiency. We also conduct comprehensive ablation studies to assess the impact of conditioning on the global shortest path and local depth features, as well as *GlocDiff*’s robustness to varying localization accuracy. Finally, we validate the practical applicability of *GlocDiff* by deploying it on an Automated Guided Vehicle (AGV) without any fine-tuning, showcasing its potential for real-world deployment.

Our contributions are summarized as follows:

- We propose conditioning the navigation policy on global path planning and local depth features to provide more effective guidance, thus enabling efficient and collision-free navigation.
- Extensive experiments validate the effectiveness and generalization of our model. Additionally, the noise injection strategy during training ensures robust adaptation to VO, leading to successful deployment on the real robot.

II. RELATED WORK

A. Mapping-based Navigation

Mapping-based navigation, the prevailing framework, requires building an environmental map first to support subsequent planning and localization. Typically, VSLAM techniques [9, 10] rely on visual observation inputs to construct sparse metric maps of the surrounding environment. In recent years, more works have started to integrate semantic information into map representations. Researchers [11–13] extract semantic categories from observations, associate the categories with each point in the point cloud, and finally generate a semantic map via differentiable projection operations and a denoising network. Other approaches integrate point-level features [14], image features [15–17], and panoramic images [18] into the built topological graph. VLFM [19] iteratively constructs an occupancy map and a value map to guide the agent toward the out-of-view target object. However, the mapping-based method has to explore unseen areas, which tends to be time-consuming for navigation. Moreover, the dynamic nature of objects in indoor environments necessitates real-time updates to the constructed map, making its reuse difficult and significantly reducing efficiency.

B. Mapless Navigation

Without relying on mapping, mapless visual navigation methods directly focus on translating observations into ac-

tions. Wjijmans et al. [20] solve the point goal navigation with a near-perfect success rate under idealized settings through large-scale reinforcement learning. Learning-based visual odometry [21, 22] is used to address realistic point goal navigation. Wenzel et al. [23] train visual-motor policies for navigation tasks in a simple 3D environment. Work [24] design a lightweight perception network and convert visual navigation to scene classification. Leveraging the diffusion policy [25], NoMaD [26] produces collision-free future actions and flexibly handle both goal-conditioned and goal-agnostic navigation via the goal masking technique. Although mapless methods eliminate the need of mapping, they often produce shortsighted actions due to the lack of global navigable information.

C. Navigation with Floor Plan

Unlike the two methods mentioned above, floorplan-based navigation eliminates the need to explore the environment and instead utilizes the inherent structure and spatial information to perform reliable navigation actions. Setalaphruk et al. [4] extract a Voronoi diagram from the sketch map and subsequently implement localization and navigation based on multiple hypotheses. Li et al. [1] propose a cognitive navigation solution using floor plans. However, its dependency on pre-collect visual features hinders its practical applicability. To eliminate the dependency, Ewe et al. [2] develop a graph-based navigation framework, enabling navigation without relying on precise scale information. Goswami et al. [6] leverage stereo-inertial sensors to construct 2D semantic point cloud, which, in conjunction with the floor plan, enables robot localization and subsequent navigation. These methods all utilize sensors other than monocular cameras. The closest related work to ours is FloNa [3], which marks the first attempt to navigate unseen environments using only a monocular camera and a floor plan. FloNa utilizes a transformer-based vision encoder to extract observation context from the floor plan and visual inputs. A diffusion policy [25], conditioned on the context, is then employed to generate actions. Although FloNa demonstrates impressive performance, it fails to effectively integrate complementary geometric clues from observations and floor plans. *GlocDiff* tackles this issue by independently processing global and local information to derive two distinct guidances.

D. Diffusion Policy

Diffusion-based policies have been successfully applied in various robotic domains, including dexterous manipulation [25, 27], locomotion [28], and path planning [3, 26]. By framing robot behavior generation as a conditional denoising diffusion process, these policies not only offer high training stability but also demonstrate strong performance in modeling complex distributions. Building upon these advances, our work focuses on utilizing diffusion policies conditioned on geometric clues derived from both visual observations and floor plans to achieve vision-based floor plan navigation.

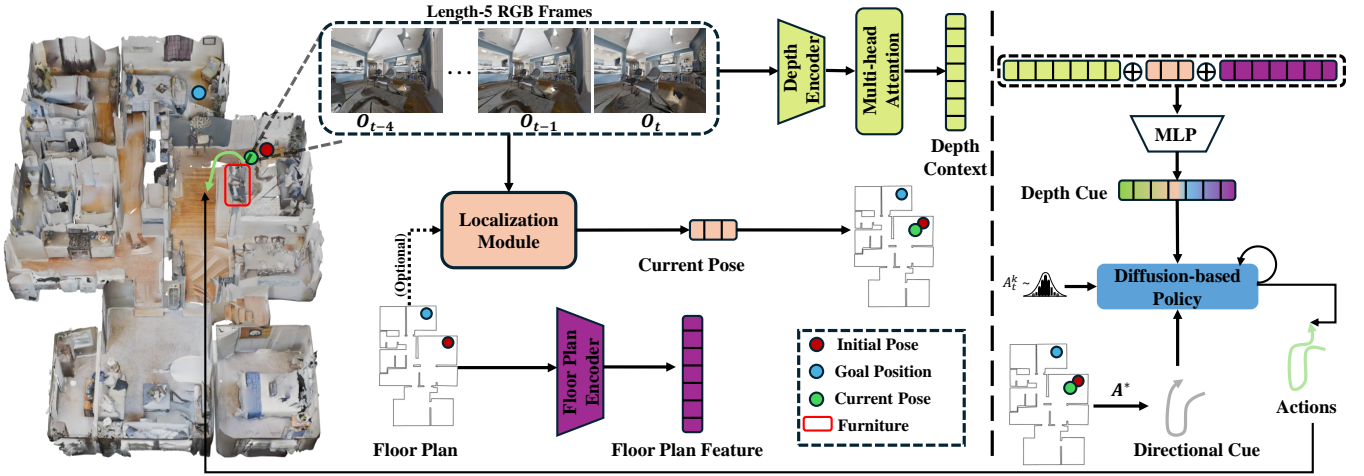


Fig. 2. **Overview of GlocDiff.** The pre-trained depth encoder uses RGB observations to produce depth latent codes, which are fed into a multi-head attention module, yielding the depth context. Taking depth context, current pose from the localization module, and floor plan feature from the floor plan encoder as inputs, the MLP outputs geometry guidance. Path planner computes the shortest path from the current position to the goal using the A* algorithm, serving as the path guidance. Conditioned on geometry and path guidance, the diffusion-based policy generates future actions.

III. METHODOLOGY

As illustrated in Fig. 2, *GlocDiff* extracts a global directional cue from the floor plan and a local depth cue primarily from the RGB observation, which together guide the diffusion policy for future action generation. In the following, we detail each key module of the proposed framework.

A. Depth Cue Module

To guide *GlocDiff* in generating collision-free actions, the depth cue module processes RGB frames and produces low-dimensional local geometric guidance.

Specifically, we employ a depth encoder [7] to extract depth features from RGB images. This encoder utilizes a latent diffusion model to model the conditional distribution $P(\mathbf{d}|\mathbf{o})$, where \mathbf{d} and \mathbf{o} denote the low-dimensional depth feature and RGB observation, respectively. In our model, the depth encoder takes 5 observations as input, including the current observation and the past 4 observations, denoted as $\mathcal{O} = \{o_{t-4}, o_{t-3}, \dots, o_t\}$. Then, the encoder outputs corresponding depth features denoted as $\mathcal{D} = \{d_{t-4}, d_{t-3}, \dots, d_t\}$. These features are then passed through the multi-head attention module [29], and the resulting fused features are averaged to derive the depth context. Subsequently, following [3], we employ a floor plan encoder consisting of an EfficientNet-B0 [30] network and a multilayer perceptron (MLP) to encode the floor plan image, obtaining a floor plan feature. Finally, the depth context, the floor plan feature, and the agent’s pose on the floor plan from the localization module (see Sec. III-B) are then concatenated and fed into an MLP to produce the local depth cue, C_l .

B. Localization Module

In our work, we employ a localization module to determine the current pose of the agent on the floor plan, p_f , using the current ego-centric observations. p_f is represented as $p_f = (q_f, r)$, where $q_f = (x_f, y_f)$ denotes the pixel

coordinate on the floor plan, and r represents the orientation. In this task, the floor plan is scaled to the environment, enabling the following equation to relate world coordinates to pixel coordinates:

$$p_w = (q_w, r) = (\mu \times x_f + \delta_x, \mu \times y_f + \delta_y, r), \quad (1)$$

where μ denotes the floor plan resolution (*i.e.*, physical distance per pixel) and δ represents the offset.

During training, we use the ground truth (GT) poses as the localization results. For testing and deployment, we utilize a visual odometry or a floor plan-based visual localization module to estimate the current pose.

C. Directional Cue Module

The directional cue module provides the policy with global shortest path guidance. Specifically, we employ the A* algorithm to compute the shortest path from the current position to the target within the floor plan. The path is represented as $\mathcal{T}_s = \{q_{f,0}, q_{f,1}, \dots, q_{f,i}, \dots, q_{f,t}\}$, where $q_{f,0}$ denotes the pixel coordinates of the current position and $q_{f,t}$ corresponds to the target point. Then, we convert each point in \mathcal{T}_s into metric coordinate using μ and δ in Eq. (1), represented as $\mathcal{T}_{w,s} = \{q_{w,0}, q_{w,1}, \dots, q_{w,i}, \dots, q_{w,t}\}$. Next, we transform each point in $\mathcal{T}_{w,s}$ to the current agent coordinate system by utilizing the formula

$$q_{a,i} = (q_{w,i} - q_{w,0}) \cdot R, \quad (2)$$

resulting in $\mathcal{T}_{a,s} = \{q_{a,0}, q_{a,1}, \dots, q_{a,i}, \dots, q_{a,t}\}$. Here, $R = \begin{pmatrix} \cos r_0 & -\sin r_0 \\ \sin r_0 & \cos r_0 \end{pmatrix}$, r_0 denotes the orientation of the first point in the shortest path. In the agent coordinate system, the agent’s current position serves as the coordinate origin, the current orientation aligns with the positive X-axis, while the leftward direction aligns with the positive Y-axis. Notably, we assume the agent does not experience height variation during navigation, and thus, we only consider a 2D coordinate system (without the Z-axis). Finally, we take the first m points of $\mathcal{T}_{a,s}$ (about 1.2 m) as the path guidance C_g .

D. Diffusion Policy

Diffusion policy [25] leverages the Denoising Diffusion Probabilistic Models (DDPMs) [31] paradigm to formulate visuomotor robot policies. In our work, using the depth and directional cues, C_l and C_g , the diffusion policy learns to approximate the conditional distribution $P(A_t|C_l, C_g)$ through a forward and reverse process, where A_t is a $m \times 2$ vector representing the generated sequence of future m actions at time step t . Each action corresponds to an approximate movement of 4 cm.

In the forward process, diffusion policy iteratively adds Gaussian noise and converts the A_t^0 to A_t^K , where A_t^0 is the initial action sequence, and K is the total steps. The entire process is given by $P(A_t^{1:K}|A_t^0) = \prod_{k=1}^K P(A_t^k|A_t^{k-1})$.

In the reverse process, diffusion policy learns the conditional distribution $P(A_t^{k-1}|A_t^k, C_l, C_g)$. Specifically, the diffusion policy employs a noise prediction network of UNet [32] architecture to predict the added noise, ϵ' , and utilizes the noise scheduler to carry out the denoising operation. The process can be described as:

$$\epsilon' = \varepsilon_\theta(A_t^k, C_l, C_g, k), \quad (3)$$

$$A_t^{k-1} = \mathcal{S}(\epsilon', A_t^k, k), \quad (4)$$

where ε denotes the noise prediction network with parameters θ and \mathcal{S} is the DDPM noise scheduler. As shown in Fig. 3, our noise prediction network includes three downsample modules, one bottleneck module, two upsample modules, and a 1D convolutional layer. Each module consists of several 1D convolutional blocks, activation functions, and residual connections. The network takes noisy actions of size $m \times 2$, along with depth and path guidance, C_l and C_g , as input and outputs a predicted noise of size $m \times 2$. C_l and the time step serve as inputs to each module. Meanwhile, C_g and the time step are first processed through two identical residual blocks, producing two features: f_1 and f_2 . f_1 is added to the output of the first residual block in the final upsample module, while f_2 is added to the output of the first residual block. Notably, we apply positional encoding to the time step before feeding it into the network. During training, we use the following loss function:

$$\mathcal{L} = \text{MSE}(\epsilon, \epsilon'), \quad (5)$$

where $\text{MSE}(\cdot)$ denotes the mean square error function, and ϵ denotes the added noise at the forward process. During inference, our model iteratively predicts and removes noise to recover a clean action sequence A_t^0 from Gaussian noise.

E. Training

We use the data provided by FloNa [3], collected from 67 Gibson simulation environments. Each scene contains 150, 180, or 200 episodes, depending on the scene size, resulting in a total of 20,214 episodes. We sample training data from this dataset, with each sample consisting of a historical observation of five consecutive RGB frames, the agent’s current position, a goal position, a floor plan image,

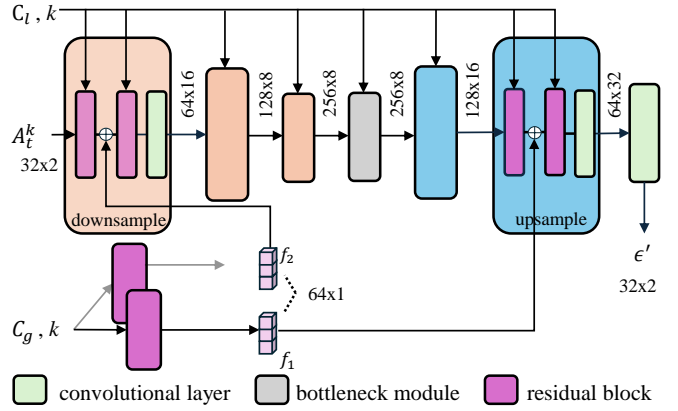


Fig. 3. **Conditional UNet.** The directional cue and the time step are fed into the first down module and the second up module, while the depth cue and the time step are fed into each module.

and the corresponding sequence of future waypoints. Unlike FloNa [3], which densely samples goal positions from future waypoints along the trajectory, we define the goal as the final waypoint of the episode. We sample one pair every five frames to avoid overlapping observations across different pairs. Consequently, our method is trained on 1.2 million samples, significantly fewer than the 180 million samples used for training Loc-FloDiff.

To improve the model’s robustness to localization noise, we introduce perturbations to both the shortest path \mathcal{T}_s and the ground truth current pose p_w during training. Specifically, we perturb the shortest path using the following formula:

$$\mathcal{T}_n = \mathcal{T}_s + u, \quad (6)$$

where \mathcal{T}_n denotes noisy path and $u \sim \mathcal{U}(0, B)$ represents the perturbation. B represents the upper bound of the perturbation, which increases with each epoch i , as shown by the following formula:

$$B_i = \alpha \cdot \sin\left(\frac{i}{N} \cdot \frac{\pi}{2}\right), \quad (7)$$

where α is the maximum perturbation value, while N represents the total epochs. Meanwhile, we add Gaussian noise, $n_p \sim \mathcal{N}(0, 0.1)$ and $n_r \sim \mathcal{N}(0, \frac{\pi}{36})$, to the ground truth position and orientation.

F. Implementation

In our implementation, the multi-head attention consists of four heads, each with four layers. We choose Square Cosine Noise Schedule [33] to train the diffusion policy. We use the AdamW optimizer, with the learning rate controlled by PyTorch’s CosineAnnealingLR scheduler. The maximum learning rate is set to 0.0001, and the maximum number of iterations is 20. We set α to 0.1. The training of **GlocDiff** is performed on 8 NVIDIA 4090 GPUs, with a batch size of 64 per GPU. **GlocDiff** is trained for $N = 20$ epochs and reaches convergence.

TABLE I

SR (%) AND SPL (%) OF DIFFERENT MODELS UNDER VARIOUS CONDITIONS. THE **BOLD** NUMBER INDICATES THE BEST RESULT.

Method		Loc-A* (GT)		DD-PPO (GT)		Map-A* (GT)		Loc-FloDiff (F ³)		Loc-FloDiff (GT)		GlocDiff (F ³)		GlocDiff (VO)		GlocDiff (GT)		
		Gibson	HM3D	Gibson	HM3D	Gibson	HM3D	Gibson	HM3D	Gibson	HM3D	Gibson	HM3D	Gibson	HM3D	Gibson	HM3D	
SR(%) ↑	τ_c	10	16.60	18.60	15.00	13.20	55.60	46.80	4.80	2.40	39.00	34.40	53.40	47.60	68.60	63.40	79.60	77.60
		30	18.20	18.80	22.80	16.40	55.60	46.80	11.60	5.20	53.40	45.80	69.20	55.80	80.80	71.80	92.80	90.40
		50	18.50	19.40	31.60	23.80	55.60	46.80	17.80	9.20	59.20	48.40	77.80	62.60	86.60	79.00	94.20	90.80
		∞	18.60	19.40	48.20	36.00	55.60	46.80	26.80	15.80	66.00	53.20	86.40	68.40	89.80	83.60	97.60	91.80
SPL(%) ↑	τ_c	10	16.50	17.44	8.40	7.80	34.23	33.79	4.02	1.54	36.30	30.60	41.67	37.85	52.88	46.84	62.62	61.24
		30	18.10	17.80	12.60	9.60	34.23	33.79	6.40	3.36	44.10	35.28	49.35	41.11	59.07	52.43	70.38	69.88
		50	18.50	18.35	16.40	13.80	34.23	33.79	8.07	5.18	46.60	37.20	52.61	47.55	61.31	55.04	70.98	70.31
		∞	18.50	18.35	23.00	18.20	34.23	33.79	9.58	8.44	48.20	40.41	54.77	49.75	62.57	56.49	72.36	71.69

TABLE II

BASELINE METHODS AND THEIR COMPONENTS.

Model	Localization	Planner	Train Set Size
Loc-A* (GT)	GT Pose	A*	-
DD-PPO (GT)	GT Pose	DD-PPO	2.5B
Map-A* (GT)	GT Pose	A*	-
Loc-FloDiff (GT)	GT Pose	Loc-FloDiff	180M
Loc-FloDiff (F ³)	F ³ Loc	Loc-FloDiff	180M
GlocDiff (F ³)	F ³ Loc	GlocDiff	1.2M
GlocDiff (GT)	GT Pose	GlocDiff	1.2M
GlocDiff (VO)	Visual Odometry	GlocDiff	1.2M

TABLE III

ERROR COMPARISON OF LOCALIZATION METHODS

localization method	Translation (m)			Orientation (°)		
	mean	median	max	mean	median	max
Visual Odometry (VO)	1.53	1.66	4.28	13.35	18.72	22.51
F ³ Loc	3.44	2.17	9.47	18.14	17.96	30.64

IV. EXPERIMENTS

We evaluate our method through comprehensive simulation experiments (including baseline comparisons and ablation studies) and subsequently deploy the policy on a physical AGV.

A. Main Experiments

a) *Setup*: We conduct our experiments in the Gibson [34] simulator. The testing scenes consist of 50 Gibson scenes and 50 HM3D [35] scenes, each containing 10 episodes. The episodes for Gibson scenes are sourced from FloNa [3], while those for HM3D scenes are newly collected under the constraint that the Euclidean distance between the start and target points exceeds 10m to ensure sufficient task difficulty. The navigation is considered successful only if the agent arrives within a distance of τ_d from the target, within the maximum step limit, and with the total number of collisions below the threshold τ_c . The agent responds to collisions by rotating 45 degrees clockwise and then re-predicting its future action sequence.

b) *Baselines*: We set eight baselines, with their specific components outlined in Tab. II. **Loc-A* (GT)**: The agent follows a path planned by the A* algorithm, with GT pose used for localization. **DD-PPO [20] (GT)**: This baseline is a reinforcement learning-based agent that navigates using only visual observations, with GT pose for localization. **Map-A***

(GT): This baseline first uses the same depth estimation model [7] as **GlocDiff** to convert RGB observations into depth. The depth is then transformed into a point cloud, which is projected to form a bird’s-eye-view (BEV) occupancy grid map. Navigation is carried out by planning a path with the A* algorithm over this occupancy map, using ground truth (GT) pose for localization. Both **Loc-FloDiff (F³)** and **GlocDiff (F³)** employ F³Loc [36], an end-to-end floor plan localization model, as their localization module. **Loc-FloDiff (GT)** and **GlocDiff (GT)**, in contrast, rely on GT pose for localization. In **GlocDiff (VO)**, a VO algorithm [8] is used to track the agent’s pose, serving as the localization module. For evaluation, we adopt Success Rate (SR) and Success Weighted by Path Length (SPL) as our metrics. We evaluate all baselines under the distance threshold τ_d values of 0.25, as well as the collision threshold τ_c values of 10, 30, 50, and ∞ .

c) *Quantitative Results*: Tab. I presents the qualitative results. Below, we discuss several key observations:

- DD-PPO (GT) and Map-A* (GT) consistently underperform **GlocDiff** (GT) across all settings. While Map-A* (GT) achieves slightly higher SR than Loc-FloDiff (GT) at $\tau_c = 10$ and 30, its SPL is lower in all cases. This suggests that incorporating a floor plan significantly improves navigation efficiency. Notably, the poor performance of DD-PPO (GT) stems from its lack of explicit obstacle-avoidance capability, combined with our collision-sensitive evaluation—unlike the setup in [20], which allows the agent to slide along obstacles.
- Despite being trained on a significantly smaller dataset, **GlocDiff** consistently outperforms Loc-FloDiff by a notable margin in both success rate and SPL, regardless of whether localization is based on GT positions or F³ Loc [36]. Moreover, when $\tau_c \geq 30$, **GlocDiff** (GT) attains a success rate above 90% and an SPL exceeding about 70%, strongly indicating that our model effectively utilizes floor plan information and exhibits robust planning capability. These outcomes validate the effectiveness and high data efficiency of our approach. Additionally, when evaluated on HM3D scenes — which differ from the Gibson scenes used in training — **GlocDiff** exhibits a smaller performance decline than Loc-FloDiff. This indicates that extracting both shortest-path guidance and depth cues from floor plans and RGB observations generalizes more robustly across varied environments compared to methods that rely

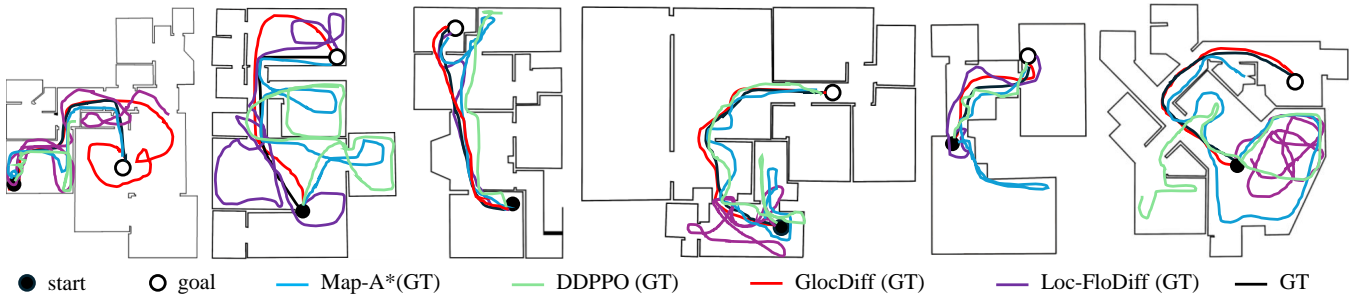


Fig. 4. **Trajectory visualization.** The visualization of trajectories for different models across six episodes.

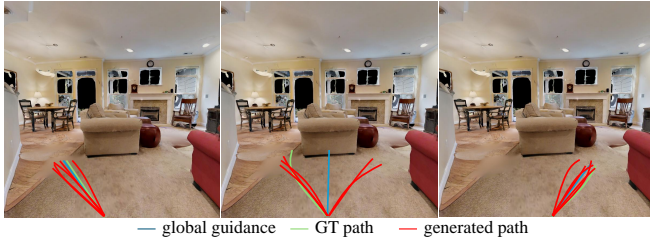


Fig. 5. Trajectory visualization of *GlocDiff* (GT) under three distinct global guidance conditions for the same observation.

- primarily on learned image features.
- When the localization results shift from GT poses to predictions from the F^3 Loc module, Loc-FloDiff experiences a significant decline in performance, with the SR dropping by 32.00% to 41.8% and the SPL decreasing by 29.06% to 38.62%. In contrast, the performance of *GlocDiff* shows a more moderate decline, with the SR falling by 11.20% to 34.60% and the SPL decreasing by 17.59% to 28.77%. This highlights that our model exhibits greater robustness to localization noise.
 - The SR of *GlocDiff* (VO) is higher than that of *GlocDiff* (F^3), with the difference being particularly pronounced under stricter collision constraints (i.e., lower τ_c). This suggests that visual odometry (VO) serves as a more suitable localization module for floor plan navigation compared to F^3 Loc. Since VO can continuously track the agent’s pose, it remains relatively stable for indoor navigation tasks, despite cumulative errors. In contrast, F^3 Loc maps observations to poses, introducing room-level errors, which is unacceptable for floor plan navigation. We further evaluate the localization accuracy of F^3 and VO. Specifically, we compute the mean and median errors between predicted and ground-truth waypoints across fifty sampled trajectories. As shown in Tab. III, VO achieves higher average accuracy than F^3 Loc. Additionally, F^3 Loc produces occasional outlier predictions, indicating abrupt jumps to distant locations in the environment.

d) *Qualitative Results:* Fig. 4 presents qualitative trajectory visualizations of Map-A* (GT), DDPPPO (GT), LocFloDiff (GT), and *GlocDiff* (GT) across six distinct scenarios. We further visualize five trajectories generated by *GlocDiff* (GT) under three different global guidance inputs

TABLE IV
ABLATION STUDY ON DIRECTIONAL AND DEPTH CUES.

Model	w/o depth		w/o path		<i>GlocDiff</i> (GT)	
	SR	SPL	SR	SPL	SR	SPL
τ_c 10	64.20	47.22	44.60	38.44	79.60	62.62
30	81.00	55.98	60.60	44.09	92.80	70.38
50	85.20	58.07	67.00	48.48	94.20	70.98
∞	92.20	60.15	73.20	50.51	97.60	72.36

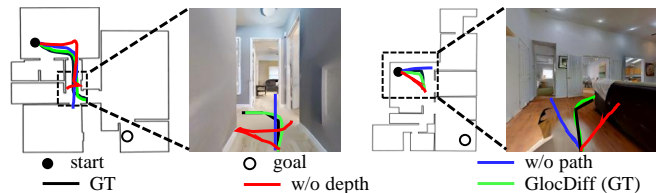


Fig. 6. **Performance of different models on the test episodes in Mobrbridge (left) and Brentsville (right).** The left column illustrates the traversed trajectory, while the right column showcases the diverse actions generated by different models based on the same observation.

for the same observation, as shown in Fig. 5. When the global guidance does not intersect with obstacles (left and right cases), *GlocDiff* (GT) consistently follows it closely across multiple runs, showing high confidence. In contrast, when the global guidance poses a collision risk with obstacles (middle case), *GlocDiff* (GT) places greater reliance on local guidance to navigate around them.

B. Ablation Study

a) *Ablation Study on Local and Global Guidances:* We further evaluate the effects of different guidances on the policy. To assess the impact of the local guidance, we use an EfficientNet to directly encode the RGB observations, obtaining RGB context to replace the original depth context, while keeping other design aspects consistent with those of *GlocDiff*. The resulting ablation model is denoted as w/o depth. To analyze the influence of the global guidance, we eliminate the global planner and directly utilize the target point to replace the shortest path, while also keeping other aspects consistent with *GlocDiff*. This modification results in another ablation model, referred to as w/o path. The two models described above are both trained for 20 epochs and reach convergence.



Fig. 7. **Three real-world test episodes.** The left columns present the top-down view of successful episodes, with 1 and 5 indicating the start and goal positions, respectively. The right columns show the AGV’s first-person RGB observations at the corresponding positions.

TABLE V

PERFORMANCE COMPARISON OF W/O PERTURBATION AND *GlocDiff*

Model		w/o perturbation		<i>GlocDiff</i>		
		SR	SPL	SR	SPL	
$u_1(m)$	τ_c	10	61.00	42.08	73.00	53.95
		30	73.00	57.15	86.00	61.86
		50	80.00	61.79	92.00	64.84
		∞	86.00	63.41	96.00	65.63
$u_2(m)$	τ_c	10	42.00	29.90	65.00	44.40
		30	52.00	34.41	69.00	52.07
		50	60.00	37.73	77.00	57.23
		∞	77.00	41.61	86.00	61.14

Quantitative results. As outlined in Tab. IV, *GlocDiff* (GT) achieves the best performance across all cases. Two key conclusions can be drawn. First, the removal of either the local guidance or the global guidance significantly degrades the model’s performance. This indicates that both global and local guidance contribute to enhancing the robot’s ability to navigate safely in complex environments. Second, w/o depth model outperforms w/o path model across SR and SPL metrics. This suggests that explicit global planning based on the floor plan provides more valuable information for efficient navigation than the local depth information derived from observations.

Qualitative results. We select two episodes, each from an unseen scene, and visualize the results in Fig. 6. When the agent navigates to the same goal, different models generate distinct actions due to their varying capabilities. The w/o depth model encounters collisions with walls and furniture in both cases, indicating the role of local guidance in generating collision-free navigation actions. In *Mobridge*, the w/o path model generates incorrect actions at the intersection due to the lack of guidance from the optimal path.

b) Ablation Study on GT Perturbation: We retrain our model removing the GT perturbation trick mentioned in Sec. III-E and refer to this revised version as w/o perturbation. To evaluate the robustness of *GlocDiff* and w/o perturbation to localization noise, we conduct a set of experiments across ten unseen environments. We introduce two levels of noise, $u_1(m) \sim \mathcal{U}(0.0, 0.5)$ and $u_2(m) \sim \mathcal{U}(0.0, 1.0)$, to the GT localization results and evaluate the performance of *GlocDiff* and w/o perturbation under both conditions.

TABLE VI

PERFORMANCE COMPARISON OF DIFFERENT PREDICTION HORIZONS

Steps	16		32		48		
	SR	SPL	SR	SPL	SR	SPL	
τ_c	10	77.40	62.69	79.60	66.60	79.00	65.00
	30	89.80	67.83	92.80	70.38	91.80	69.09
	50	94.00	68.62	94.20	70.98	94.40	70.32
	∞	97.80	71.89	97.60	72.36	97.40	72.23

As shown in Tab. V, under noisy ground-truth localization, *GlocDiff* consistently outperforms w/o perturbation in most scenarios. This indicates that incorporating noise during training significantly enhances the model’s robustness to localization errors.

c) Ablation Study on Prediction Horizon: We examine how different action prediction horizons affect the performance of *GlocDiff* (GT). Specifically, we evaluate three configurations with prediction lengths of 16, 32, and 48 steps. All models are trained for 20 epochs until convergence. We evaluate all three models using a fixed distance threshold $\tau_d = 0.25$, and vary the intervention count threshold τ_c among 10, 30, 50, ∞ . According to Tab. VI, all three configurations yield comparable performance, with the 32-step model performing slightly better.

C. Real World Deployment

This section presents the results of deploying the *GlocDiff* on an AGV in a real apartment without any fine-tuning. The AGV is equipped with a mobile base, an RGB camera, and an NVIDIA Jetson AGX Orin for model execution. To ensure stable performance, we utilize the AGV’s single-line LiDAR-based odometry for pose estimation, with the robot’s initial pose pre-calibrated. On the Orin device, the model achieves an inference speed of approximately 1.21Hz. The actions generated by *GlocDiff* are converted into linear and angular velocities via a PD controller.

We evaluate the system over 10 episodes with $\tau_c = 0$ and $\tau_d = 20\text{cm}$. Each pair is tested three times to ensure reliability, yielding a final success rate of 40%. Fig. 7 presents three navigation episodes, demonstrating the generalization of obstacle avoidance and planning to unseen real-world environments. Please refer to the accompanying demo for a more intuitive illustration.

V. CONCLUSION

In summary, we propose an efficient and practical visual navigation framework based on floor plans, leveraging local and global condition extraction alongside a diffusion policy. Our method addresses the challenge of efficiently integrating visual information with floor plan for optimal path planning. Meanwhile, visual odometry ensures stable localization, enhancing real-world applicability. Looking forward, we foresee the integration of multi-modal data, such as language or object information, further improving adaptability and robustness, paving the way for intelligent indoor service robots in complex environments.

REFERENCES

- [1] J. Li, C. L. Chan, J. Le Chan, Z. Li, K. W. Wan, and W. Yun Yau, "Cognitive navigation for indoor environment using floorplan," in *International Conference on Intelligent Robots and Systems (IROS)*, 2021.
- [2] Z. L. Ewe, F.-H. Chang, Y.-S. Huang, and L.-C. Fu, "Spatial graph-based localization and navigation on scaleless floorplan," *IEEE Robotics and Automation Letters (RA-L)*, vol. 9, no. 4, pp. 3932–3939, 2024.
- [3] J. Li, W. Huang, Z. Wang, W. Liang, H. Di, and F. Liu, "Flona: Floor plan guided embodied visual navigation," in *AAAI Conference on Artificial Intelligence (AAAI)*, 2025.
- [4] V. Setalaphruk, A. Ueno, I. Kume, Y. Kono, and M. Kidode, "Robot navigation in corridor environments using a sketch floor map," in *International Symposium on Computational Intelligence in Robotics and Automation*, 2003.
- [5] L. Ericson and P. Jensfelt, "Beyond the frontier: Predicting unseen walls from occupancy grids by learning from floor plans," *IEEE Robotics and Automation Letters (RA-L)*, vol. 9, no. 8, pp. 6832–6839, 2024.
- [6] R. Goswami, H. Sinha, P. Amith, J. Hari, P. Krishnamurthy, J. Rizzo, and F. Khorrami, "Floor plan based active global localization and navigation aid for persons with blindness and low vision," *IEEE Robotics and Automation Letters (RA-L)*, vol. 9, no. 12, pp. 11 058–11 065, 2024.
- [7] B. Ke, A. Obukhov, S. Huang, N. Metzger, R. C. Daudt, and K. Schindler, "Repurposing diffusion-based image generators for monocular depth estimation," in *Conference on Computer Vision and Pattern Recognition (CVPR)*, 2024.
- [8] F. Luigi, "pySLAM: An open-source, modular, and extensible framework for visual slam," 2025. [Online]. Available: <https://github.com/luigifreda/pyslam>
- [9] R. Mur-Artal, J. M. M. Montiel, and J. D. Tardós, "Orb-slam: A versatile and accurate monocular slam system," *Transactions on Robotics (T-RO)*, vol. 31, no. 5, pp. 1147–1163, 2015.
- [10] R. Mur-Artal and J. D. Tardós, "Orb-slam2: An open-source slam system for monocular, stereo, and rgb-d cameras," *Transactions on Robotics (T-RO)*, vol. 33, no. 5, pp. 1255–1262, 2017.
- [11] D. S. Chaplot, D. P. Gandhi, A. Gupta, and R. R. Salakhutdinov, "Object goal navigation using goal-oriented semantic exploration," in *Advances in Neural Information Processing Systems (NeurIPS)*, 2020.
- [12] S. K. Ramakrishnan, D. S. Chaplot, Z. Al-Halah, J. Malik, and K. Grauman, "Poni: Potential functions for objectgoal navigation with interaction-free learning," in *Conference on Computer Vision and Pattern Recognition (CVPR)*, 2022.
- [13] Y. Guo, J. Sun, R. Zhang, Z. Jiang, Z. Mi, C. Yao, X. Ban, and M. S. Obaidat, "An object-driven navigation strategy based on active perception and semantic association," *IEEE Robotics and Automation Letters (RA-L)*, vol. 9, no. 8, pp. 7110–7117, 2024.
- [14] C. Huang, O. Mees, A. Zeng, and W. Burgard, "Visual language maps for robot navigation," in *International Conference on Robotics and Automation (ICRA)*, 2023.
- [15] H. Yoo, Y. Choi, J. Park, and S. Oh, "Commonsense-aware object value graph for object goal navigation," *IEEE Robotics and Automation Letters (RA-L)*, vol. 9, no. 5, pp. 4423–4430, 2024.
- [16] S. Chen, P.-L. Guhur, M. Tapaswi, C. Schmid, and I. Laptev, "Think global, act local: Dual-scale graph transformer for vision-and-language navigation," in *Conference on Computer Vision and Pattern Recognition (CVPR)*, 2022.
- [17] H. Wang, W. Liang, L. Van Gool, and W. Wang, "Dreamwalker: Mental planning for continuous vision-language navigation," in *International Conference on Computer Vision (ICCV)*, 2023.
- [18] D. S. Chaplot, R. Salakhutdinov, A. Gupta, and S. Gupta, "Neural topological slam for visual navigation," in *Conference on Computer Vision and Pattern Recognition (CVPR)*, 2020.
- [19] N. Yokoyama, S. Ha, D. Batra, J. Wang, and B. Bucher, "Vlfm: Vision-language frontier maps for zero-shot semantic navigation," in *International Conference on Robotics and Automation (ICRA)*, 2024.
- [20] E. Wijmans, A. Kadian, A. Morcos, S. Lee, I. Essa, D. Parikh, M. Savva, and D. Batra, "Dd-ppo: Learning near-perfect pointgoal navigators from 2.5 billion frames," in *International Conference on Learning Representations (ICLR)*, 2020.
- [21] R. Partsey, E. Wijmans, N. Yokoyama, O. Doboševych, D. Batra, and O. Maksymets, "Is mapping necessary for realistic pointgoal navigation?" in *Conference on Computer Vision and Pattern Recognition (CVPR)*, 2022.
- [22] X. Zhao, H. Agrawal, D. Batra, and A. G. Schwing, "The surprising effectiveness of visual odometry techniques for embodied pointgoal navigation," in *International Conference on Computer Vision (ICCV)*, 2021.
- [23] P. Wenzel, T. Schön, L. Leal-Taixé, and D. Cremers, "Vision-based mobile robotics obstacle avoidance with deep reinforcement learning," in *International Conference on Robotics and Automation (ICRA)*, 2021.
- [24] T. Ran, L. Yuan, and J. Zhang, "Scene perception based visual navigation of mobile robot in indoor environment," *ISA Transactions*, vol. 109, pp. 389–400, 2021.
- [25] C. Chi, S. Feng, Y. Du, Z. Xu, E. Cousineau, B. Burchfiel, and S. Song, "Diffusion policy: Visuomotor policy learning via action diffusion," in *Robotics: Science and Systems (RSS)*, 2023.
- [26] A. Sridhar, D. Shah, C. Glossop, and S. Levine, "Nomad: Goal masked diffusion policies for navigation and exploration," in *International Conference on Robotics and Automation (ICRA)*, 2024.
- [27] A. Simeonov, A. Goyal, L. Manuelli, L. Yen-Chen, A. Sarmiento, A. Rodriguez, P. Agrawal, and D. Fox, "Shelving, stacking, hanging: Relational pose diffusion for multi-modal rearrangement," in *Conference on Robot Learning (CoRL)*, 2023.
- [28] X. Huang, Y. Chi, R. Wang, Z. Li, X. B. Peng, S. Shao, B. Nikolic, and K. Sreenath, "Diffuseloco: Real-time legged locomotion control with diffusion from offline datasets," *arXiv preprint arXiv:2404.19264*, 2024.
- [29] A. Vaswani, N. Shazeer, N. Parmar, J. Uszkoreit, L. Jones, A. Gomez, L. Kaiser, and I. Polosukhin, "Attention is all you need," in *Advances in Neural Information Processing Systems (NeurIPS)*, 2017.
- [30] M. Tan and Q. Le, "Efficientnet: Rethinking model scaling for convolutional neural networks," in *International Conference on Machine Learning (ICML)*, 2019.
- [31] J. Ho, A. Jain, and P. Abbeel, "Denosing diffusion probabilistic models," in *Advances in Neural Information Processing Systems (NeurIPS)*, 2020.
- [32] O. Ronneberger, P. Fischer, and T. Brox, "U-net: Convolutional networks for biomedical image segmentation," in *International Conference on Medical Image Computing and Computer-Assisted Intervention (MICCAI)*, 2015.
- [33] A. Q. Nichol and P. Dhariwal, "Improved denosing diffusion probabilistic models," in *International Conference on Machine Learning (ICML)*, 2021.
- [34] F. Xia, A. R. Zamir, Z. He, A. Sax, J. Malik, and S. Savarese, "Gibson env: Real-world perception for embodied agents," in *Conference on Computer Vision and Pattern Recognition (CVPR)*, 2018.
- [35] S. K. Ramakrishnan, A. Gokaslan, E. Wijmans, O. Maksymets, A. Clegg, J. M. Turner, E. Undersander, W. Galuba, A. Westbury, A. X. Chang, M. Savva, Y. Zhao, and D. Batra, "Habitat-matterport 3d dataset (HM3d): 1000 large-scale 3d environments for embodied AI," in *Thirty-fifth Conference on Neural Information Processing Systems Datasets and Benchmarks Track (Round 2)*, 2021.
- [36] C. Chen, R. Wang, C. Vogel, and M. Pollefeys, "F³loc: Fusion and filtering for floorplan localization," in *Conference on Computer Vision and Pattern Recognition (CVPR)*, 2024.